March 31st, 2023

Blocking Interleukin-1β transiently limits left ventricular dilation and modulates cardiac lymphangiogenesis in a mouse pressure-overload model

Heron C.[1], Lemarcis T.[1], Laguerre O.[1], Valet M.[1], Michel JB.[2], Mulder P.[1], Tardif V.[1], *Brakenhielm E.[1]

[1] UnivRouen Normandie, INSERM EnVI, UMR1096, France
[2] UMR 1148, Inserm-Paris University, X. Bichat Hospital, Paris, France

Keywords: Hypertrophy, inflammation, lymphatics, VEGF-C, perivascular fibrosis

Running title: Cardiac and lymphatic impact of anti-IL-1β treatment

Abstract	249 words
Main text, references and legends	6 486 words
Figures & Tables	5+ 1
Suppl. Figs & Tables	4 + 4
References	38

***Corresponding authors**:
Dr. Ebba Brakenhielm, Inserm UMR1096, Normandy University, UniRouen, Faculty of Medicine, 22 Boulevard Gambetta, 76183 Rouen, France

Dr. Virginie Tardif, Inserm UMR1096, Normandy University, UniRouen, Faculty of Medicine, 22 Boulevard Gambetta, 76183 Rouen, France

Tel. +33-235-148370; Fax +33-235-148365; email: ebba.brakenhielm@inserm.fr
ORCID: https://orcid.org/0000-0003-3378-8300

The authors declare that no conflict of interest exists

Abstract

Blocking inflammatory pathways, such as the inflammasome or IL-1β, is a promising therapeutic target in both ischemic and non-ischemic heart failure (HF). We hypothesize that IL-1β may stimulate cardiac lymphangiogenesis, driven by left ventricular dilation in HF. Thus, blocking IL-1β signaling may reduce lymphangiogenesis, which could delay resolution of myocardial edema and inflammation, aggravate cardiac fibrosis, and accelerate HF development.

Here, we investigated the effects of *early* versus *late* anti-IL-1β treatment during pressure-overload induced by transaortic constriction (TAC) in Balb/c mice prone to left ventricular (LV) dilation. We also investigated links between perivascular lymphatics and fibrosis in ischemic versus dilated cardiomyopathy (DCM) HF patients.

We found that *early* treatment transiently delayed LV dilation, but did not alter cardiac hypertrophy or dysfunction at 8 weeks post-TAC. *Late* treatment reduced cardiac lymphangiogenesis and lymphatic CCL21 gradients. Surprisingly, cardiac inflammation, fibrosis and dysfunction were not aggravated despite reduced lymphatic density. Further, similar as in mice, increased perivascular lymphatic density in HF patients was associated with less perivascular fibrosis.

In conclusion, we found limited functional cardiac benefit of IL-1β blockage when initiated before onset of lymphangiogenesis post-TAC in Balb/c mice. In contrast, *late* treatment reduced cardiac lymphangiogenesis. HF onset was however not significantly accelerated, likely reflecting lymphatic transport dysfunction post-TAC. Taken together, the therapeutic window for anti-IL-1β treatment appears crucial, as initiation of treatment during the lymphangiogenic response, induced by LV dilation, may limit the potential cardiac benefit in HF patients. Further, our data indicate that IL-1β-independent perivascular lymphangiogenesis may limit perivascular fibrosis.

Introduction

Blockage of Interleukin-1β (IL-1β) signaling has emerged as a promising therapeutic target to limit inflammation in cardiovascular diseases, as highlighted in the CANTOS study, where Canakinumab reduced major adverse cardiovascular events in atherosclerotic patients.[1] Currently, other anti-IL-1β treatments, such as *Anakinra*, are being evaluated in the setting of ischemic heart failure (HF)[2]. Interestingly, IL-1β protein levels are increased also in non-ischemic dilated cardiomyopathy (DCM) HF patients.[3] However, few experimental studies have investigated the cardiac impact of targeting IL-1β in non-ischemic cardiomyopathy, such as following pressure-overload induced by transverse aortic constriction (TAC).

IL-1β not only regulates inflammation and fibrosis (in part by stimulating IL-6), but it also impacts cardiac function *directly* due to negative inotropic effects.[4] In addition, IL-1β may stimulate cardiomyocyte hypertrophy *via* upregulation of *Igf1*[5]. Promisingly, reduction of cardiac IL-1β production during pressure-overload, by *early* treatment with a selective pharmacological NLRP3 inflammasome inhibitor, reduced both cardiac hypertrophy and fibrosis at 5 weeks post-TAC in male C57Bl/6J mice.[6] However, another study, employing an IL-1β-blocking antibody post-TAC in male C57Bl/6J, demonstrated that the reduction of left ventricular (LV) hypertrophy accelerated LV dilation and dysfunction.[7] Notably, this aggravation of HF development was linked to reduced TAC-induced VEGF-A-mediated cardiac angiogenesis. Similarly, a recent study, based on NLRP3 gene deletion in male C57Bl/6J mice, revealed that prevention of the early compensatory cardiac hypertrophy response post-TAC accelerated LV dilation and aggravated cardiac dysfunction.[8] Thus, the potential of IL-1β as a therapeutic target to limit HF development in non-ischemic cardiomyopathy currently remains uncertain.

Recently, we demonstrated that while pressure-overload leads to compensated concentric hypertrophy in female C57Bl/6J mice, in Balb/c mice, characterized by elevated cardiac *Il1b* gene expression post-TAC, it leads to eccentric hypertrophy with severe LV dilation.[9] Moreover, we demonstrated that LV dilation-induced wall stress, but not LV hypertrophy, triggers massive cardiac lymphangiogenesis, which however fails to limit cardiac inflammation and edema.[9] Lymphatics are essential for cardiac function, and consequently cardiac lymphatic dysfunction or insufficient lymphangiogenesis has been shown experimentally to contribute to adverse cardiac

remodeling, inflammation, and fibrosis following myocardial infarction or pressure-overload.[10–15] Conversely, inflammatory mediators, including IL-1β, may modulate lymphangiogenesis and/or lymphatic function.[16–18] Interestingly, we previously observed a striking correlation between cardiac *Il1b* and *Vegfc* expression[9], in line with previous published reports in tumors demonstrating both direct and indirect pro-lymphangiogenic effects of IL-1β[16]. This includes stimulation of VEGF-C-mediated proliferation of lymphatic endothelial cells (LEC) *via* an autocrine loop, as well as IL-1β-mediated activation of VEGF-C-release by macrophages to promote lymphangiogenesis during chronic inflammation in other tissues[19]. In contrast, tissue inflammation induces lymphatic dysfunction, as pro-inflammatory mediators, including IL-1β, act on lymphatic smooth muscle cells to reduce lymphatic drainage.[20] Additionally, in the heart, where lymphatic drainage depends directly on the force of cardiac contraction[21], the negative inotropic effects of IL-1β[4] may contribute to cardiac lymphatic dysfunction in cardiovascular diseases.

Here, we investigated the impact of anti-IL-1β treatment on cardiac lymphatics and HF development at 8 weeks post-TAC in Balb/c mice prone to LV dilation. We hypothesized that elevated cardiac *Il1b* may provide a molecular link between increased wall stress and cardiac lymphangiogenesis during pressure-overload. Specifically, we argued that the striking lymphangiogenesis post-TAC in Balb/c mice may be induced by elevated cardiac IL-1β levels. This would mechanistically couple cardiac wall stress (induced by LV dilation) to local VEGF-C production, as cardiac fibroblast secretion of IL-1β is sensitive to mechanical stress.[5] We expected that interfering with IL-1β signaling in Balb/c mice post-TAC would have deleterious effects including *i)* reduction of compensatory cardiac hypertrophy leading to accelerated LV dilation; and *ii)* reduction of cardiac angiogenesis and lymphangiogenesis leading to aggravated inflammation and fibrosis. To investigate the cardiac functional and lymphatic impact of IL-1β in different stages of pressure-overload-induced HF, we applied an anti-IL-1β antibody (*Gevokizumab*) before and after development of LV dilation in Balb/c (*early* and *late* treatment, **Fig. 1a**).

Results

Early, but not late, anti-IL-1β treatment delays LV dilation and dysfunction but does not limit HF development post-TAC.

Evaluation of cardiac function by echocardiography at 3-, 6-, and 8 weeks post-TAC unexpectedly demonstrated that *early* anti-IL-β treatment prevented LV dilation and dysfunction up to 6 weeks-post-TAC (**Fig. 1b-e**; **Table 1**; **Suppl. Table 1**). Indeed, the reduction in LV hypertrophy index, observed in TAC controls starting from 3 weeks, was delayed in *early*-treated mice (**Fig. 1e**). However, at the end of the study, this beneficial functional cardiac effect was lost, and treated animals displayed similar reduction of fractional shortening (FS) as compared to control TAC mice (**Fig. 1d**). Moreover, morphometry and gravimetry measurements did not reveal any effects of *early*-stage treatment on TAC-induced cardiac hypertrophy (**Fig. 1f; Suppl. Fig. 1**) or pulmonary edema (**Fig. 1g**) evaluated at 8 weeks post-TAC.

In contrast, *late* anti-IL-β treatment tended to increase LV dilation (**Fig. 1b, Table 1**), although it did not significantly aggravate cardiac dysfunction, hypertrophy, or pulmonary edema at 8 weeks (**Fig. 1d-g**). Moreover, cardiac gene expression of *Nppa* and *Nppb* were similarly increased, as compared to TAC controls, at 8 weeks post-TAC in both *early* and *late* treated mice (**Fig. 1h**). Evaluation of cardiomyocytes sizes similarly revealed moderate cardiac hypertrophy at 8 weeks post-TAC, which was unaltered by anti-IL-β treatment (**Fig. 1j**).

Only *early* anti -IL-1β treatment moderately affects cardiac inflammation post-TAC

We and others have previously shown biphasic upregulation of cardiac IL-1β during experimental pressure-overload, with a rapid increase (from 3 days post-TAC[21]), followed by a second progressive increase (from 3 to 8 weeks post-TAC).[9,22] Pressure-overload not only activates inflammatory pathways in the heart, but also systemic innate immune cell activation, which in the chronic setting leads to splenomegaly. [22,23] We found that both *early* and *late* anti-IL-1β treatment significantly reduced spleen weight at 8 weeks post-TAC (**Fig. 2a**), reflecting systemic anti-inflammatory effects of the treatment, as we previously described in rats.[24] Only *late* anti-IL-1β treatment led to compensatory increase in circulating IL-1β plasma levels, as evaluated by ELISA (**Fig. 2b**). Of note, rather than neutralizing the cytokine, *Gevokizumab* acts by reducing IL-1β binding to IL-1R receptor.[24] In contrast, neither *early* or *late* treatment altered IL-

1β cardiac protein or gene expression levels post-TAC (**Fig. 2c, d**). Unexpectedly, anti-IL-1β treatment did not reduce cardiac gene expression of other proinflammatory cytokines, including *Il6* and *Il33*, evaluated by qPCR, as compared to control TAC mice (**Fig. 2e**). Of note, all three cytokines, and notably *Il6*, correlated with the degree of LV dilation at 8 weeks post-TAC (**Suppl. Fig. 2**).

Concerning the impact of the treatment on cardiac immune cell levels, neither *early* or *late* treatment significantly altered total macrophage levels (**Fig. 2f**). However, *early* anti-IL-1β treatment tended to reduce cardiac-infiltrating $CD68^+$ / Lyve-1^- macrophages at 8 weeks post-TAC, as evaluated by immunohistochemistry (**Fig. 2g**). In contrast, neither treatment significantly altered residential $CD68^+$/Lyve-1^+ macrophage expansion post-TAC (**Fig. 2h, i**).

Taken together, the limited benefit of *early* anti-IL-1β treatment on cardiac inflammation is in line with the transient and moderate improvement of cardiac dysfunction post-TAC seen in our study. In contrast, our findings that *late* anti-IL-1β treatment did not suffice to block cardiac inflammation following pressure-overload indicate that other pro-inflammatory cytokines induced by cardiac wall stretch, such as IL-6[4], may counteract reduced IL-1β signaling, notably in the decompensated phase post-TAC.

Anti-IL-1β treatments alters cardiac lymphangiogenesis post-TAC.

We previously demonstrated that cardiac *Vegfc* gene expression is increased starting from 3-4 weeks post-TAC in Balb/c mice, stimulating cardiac lymphangiogenesis during the subsequent rapid LV dilation in the decompensation phase (6-8 weeks post-TAC).[9] Using western blot of cardiac samples at 8 weeks post-TAC, we found that VEGF-C protein levels, specifically the ratio between mature and immature forms of the protein, were significantly increased post-TAC as compared to sham mice (**Fig. 3a**), while VEGF-D protein levels were not altered (**Suppl. Fig. 3a**). These results confirm our previous findings that cardiac lymphangiogenesis post-TAC in Balb/c mice is essentially mediated by VEGF-C.[9] Further, our new data suggest that enhanced maturation of VEGF-C may occur post-TAC in Balb/c mice. Interestingly, we observed subpopulation-dependent correlation between cardiac macrophage densities and lymphatic densities post-TAC, with infiltrating macrophages potentially exerting deleterious impact while residential macrophages were linked to enhanced

lymphangiogenesis (**Suppl. Fig. 3b, c**). Indeed, residential macrophages have recently been proposed as a preferential source of VEGF-C in the heart. [25]

Consequently, as *early* anti-IL-1β treatment reduced infiltrating macrophage levels, we found that it potentiated lymphatic capillary expansion at 8 weeks (**Fig. 3b, Suppl. Fig. 4**). However, the treatment did not increase cardiac VEGF-C levels (**Fig. 3a**), open vessel densities or sizes at 8 weeks post-TAC (**Fig. 3c, d**). Moreover, cardiac gene expression analysis revealed that *early* anti-IL-1β treatment did not alter expression levels of key lymphatic markers and regulators (*Pdpn*, *Ccl21*, *Lyve1*, *Vegfc*, and *Vegfd*) as compared to control TAC mice (**Suppl. Table 2**).

Secondly, in agreement with our hypothesis of a role of IL-1β in linking LV dilation and lymphangiogenesis, we found that *late* anti-IL-1β, initiated at 4 weeks post-TAC, before LV dilation, potently reduced cardiac levels of mature VEGF-C (**Fig. 3a**), leading to reduced lymphangiogenesis at 8 weeks (**Fig. 3b, c, Suppl. Fig. 4**) despite similar LV dilation in *late*-treated and TAC control groups (**Fig. 1b, c**). Interestingly, while both lymphatic capillary and precollector densities were reduced, lymphatic vessel sizes were increased (**Fig. 3d**). This enlargement of lymphatics ("profile switch" from 5-20 µm size range to 20-50 µm vessel diameters (**Suppl. Fig. 3d**)) was sufficient to compensate for the reduction in lymphangiogenesis following anti-IL-1β treatment, and total cardiac lymphatic areas remained unchanged, as compared to TAC controls (**Fig. 3e**). In contrast, coronary perivascular lymphatic density, increased post-TAC, was not altered by either *early* or *late* anti-IL-1β treatment (**Fig. 3f**).

Although cardiac expression analyses indicated that *late* anti-IL-1β treatment reduced *Vegfd* levels (**Suppl. Table 1**), western blot analyses of VEGF-D did not confirm this (**Suppl. Fig. 3a**). Further, despite the reduced lymphatic density, we found that *late* anti-IL-1β treatment increased cardiac *Lyve1* and *Ccl21* gene expression levels, as compared to control TAC mice (**Suppl. Table 2**). However, immunohistochemical analyses revealed that CCL21 lymphatic gradients were not increased, but paradoxically decreased in *late*-treated mice (**Fig. 3g, h**). Notably, reduced CCL21 gradients may limit lymphatic drainage of $CCR7^+$ immune cells, including macrophages. However, as noted previously, we did not observe any increase in cardiac macrophage levels at 8 weeks post-TAC in *late* anti-IL-1β-treated TAC mice. Thus, the mechanisms, and functional relevance, of reduced cardiac CCL21 gradients in *late* anti-IL-1β-treated mice remain to be investigated. Moreover, given these

discrepancies noted between cardiac gene and protein expression levels in *late* anti-IL-1β-treated mice, it is tempting to speculate that inhibition of IL-1β may have influenced cardiac processes related to protein maturation, such as reduced activity of specific proteases targeting VEGF-C, VEGF-D, and CCL21.[26,27]

Early, but not late, anti-IL-1β treatment modulates cardiac fibrosis post-TAC

Cardiac inflammation and edema, if unresolved by poor lymphatic drainage from the cardiac interstitium, may aggravate cardiac fibrosis.[21] Our recent study highlighted that while interstitial fibrosis was elevated at 8 weeks post-TAC in Balb/c mice, they were protected against perivascular fibrosis, as compared with C57Bl/6J mice.[9] We proposed that this may be due to expansion of perivascular lymphatics in the former.[9] In support, we found a significant negative correlation between the extent of coronary perivascular fibrosis and perivascular lymphatic densities in mice (**Fig. 4a**). This suggests that cardiac lymphangiogenesis during pressure-overload may prevent perivascular fibrosis locally, despite generalized lymphatic dysfunction in the heart contributing to unresolved inflammation and edema stimulating interstitial fibrosis post-TAC. Similarly, we previously reported increased lymphatic density around coronaries in clinical biopsies from HF patients, especially in the setting of DCM.[9] Histological analyses revealed that this was associated with lower levels of perivascular fibrosis in DCM patients as compared to those with ischemic HF (**Fig. 4b, c**), as evaluated in similar sized arterioles (**Fig. 4d, e**). Interestingly, while our study is the first to show negative correlation between perivascular lymphatics and fibrosis, previous studies have similarly reported low levels of perivascular fibrosis in DCM patients.[28]

In our experimental study, we found that while *early* anti-IL-1β treatment slightly reduced cardiac-infiltrating macrophages, it unexpectedly increased interstitial fibrosis as compared to control TAC mice (**Fig 4f**). This would suggest potential beneficial effects of IL-1β in limiting profibrotic mechanisms in the semi-acute phase (1-5 weeks) post-TAC likely related to the balance between hypertrophy and LV dilation. Indeed, as *early* blockage of IL-1β during pressure-overload delayed LV dilation post-TAC, accelerated changes in LV wall stress occurring in the chronic phase may have contributed to aggravate interstitial fibrosis by hyper-activating mechanical-stress responses in LV fibroblasts. In contrast, neither *early* or *late* anti-IL-1β treatment altered TAC-induced development of replacement fibrosis (micro-scars) or

perivascular fibrosis (**Fig. 4g, h**), as evaluated in 16-60μm in diameter coronary vessel segments (**Fig. 4i**).

Discussion

In this study, we demonstrated that anti-IL-1β treatment with *Gevokuzimab* during pressure-overload did not significantly alter chronic cardiac inflammation, nor was it sufficient to durably prevent deleterious cardiac remodeling, fibrosis, or HF development post-TAC in Balb/c mice. In contrast, in line with our hypothesis, we found that IL-1β appears to play a key role in the lymphangiogenic response induced by LV dilation. This lymphatic expansion is triggered in the chronic stage following pressure-overload, between 4-8 weeks post-TAC in Balb/c mice. Our data demonstrate that *late* anti-IL-1β treatment reduced TAC-induced cardiac lymphangiogenesis, without altering cardiac macrophage levels or *Vegfc* gene expression in the heart. Instead, our data show reduced mature VEGF-C protein levels in *late*-treated TAC mice. In contrast, *early* anti-IL-1β treatment, discontinued week-5 post-TAC, did not reduce cardiac lymphangiogenesis. Indeed, surprisingly, it slightly increased lymphatic capillary, but not precollector, densities. Potentially, this reflects deleterious impact of infiltrating macrophages, reduced by *early* anti-IL-1β treatment, on cardiac lymphangiogenesis during pressure-overload. Alternatively, as LV dilation was transiently delayed up to 6 weeks post-TAC, it is possible that the subsequent accelerated increase in cardiac wall stress upon termination of treatment may have led to increased *Vegfc* expression in *early* treated mice. However, at 8 weeks, we did not find any differences in cardiac lymphangiogenic growth factor gene or protein levels in *early*-treated mice versus TAC controls. Another potential mechanism is that cardiac IL-1β may exert deleterious effects on lymphatic function post-TAC before the onset of lymphangiogenesis. This may contribute to enhance lymphatic capillary reactivity to lymphangiogenic factors in *early*-treated mice, despite similar lymphangiogenic stimuli in the decompensating phase post-TAC. Further studies are needed to investigate this possibility.

The pro-lymphangiogenic effects of IL-1β may be *indirect*, as previously described in mice with tracheal *Il1b*-overexpression.[19] In this setting, blockage of VEGF-C/-D signaling, with soluble VEGFR-3, inhibited the pro-lymphangiogenic effects of IL-1β, demonstrating its dependency on the VEGFR-3 axis. The authors further demonstrated that IL-1β stimulated tissue-recruitment of macrophages, and increased their release of VEGF-C. In contrast, we found negative correlation between infiltrating cardiac macrophages and lymphatic densities post-TAC. Thus, in our study, cardiac

IL-1β did not stimulate lymphangiogenesis post-TAC by promoting cardiac recruitment of macrophages. Instead, in line with a previous report in C57Bl/6 mice [25], we found weak, but positive, correlation between densities of residential cardiac macrophages and lymphatics. However, IL-1β does not appear as a major regulator of LYVE1$^+$ residential cardiac macrophages, as neither *early* or *late* phase blockage of IL-1β post-TAC altered densities of this subpopulation. Another potential mechanism of IL-1β is *direct* activation of LECs *via* IL-1R1.[29] This would enhance LEC NFκB signaling, promoting increased *Vegfr3* expression thus sensitizing LECs to VEGF-C produced in autocrine or paracrine manners[29]. However, our unpublished molecular analyses have revealed that only 1-2% of cardiac LECs express IL-1R1, and this was not altered after TAC. A third possibility is that IL-1β may influence VEGF-C maturation by altering the expression or activity of extracellular proteases in the heart, such as Plasmin, Adamts3, or Thrombin.[26] Of note, inhibition of IL-1β signaling in the clinic has been suggested to reduce tissue plasminogen activator plasma levels.[30]

In addition to stimulating VEGF-C-mediated lymphangiogenesis post-TAC, our data suggest that IL-1β may influence lymphatic immune function by stimulating CCL21 release by LECs. Interestingly, while cardiac *Ccl21* gene expression was increased in *late* anti-IL-1β treated mice, we show that lymphatic CCL21 chemokine gradients were reduced. This is expected to limit immune cell drainage from the heart, slowing inflammatory resolution. Indeed, CCL21 is the main chemokine released by lymphatics and its receptor, CCR7, is expressed on both lymphoid and myeloid cells [31-32]. Our *in silico* analysis of recent single cell RNA sequencing (scRNAseq) data on cardiac-infiltrating immune cells from C57Bl/6J mice post-TAC[33] indicate that in the heart, both B and T cells have elevated *Ccr7* expression. We previously showed, by flow cytometry in Balb/c mice at 8 weeks post-TAC, that cardiac B cell levels are low but there is a retention of macrophages and T cells.[9] Thus, reduced lymphatic CCL21 levels, together with reduced lymphatic density following inhibition of IL-1β, could potentially increase cardiac B or T cell retention post-TAC. In contrast, we expected that anti-IL-1β treatment, by limiting local inflammatory processes in the heart, would limit pro-inflammatory macrophage infiltration post-TAC, and increase residential macrophage proliferation, known to be cardioprotective post-TAC.[25] However, we found no differences in residential CD68$^+$/Lyve-1$^+$ macrophage levels in either *early* or *late*-treated groups. Further, only *early* anti-IL-1β treatment led to a decrease in cardiac-

infiltrating CD68^{+}/Lyve-1^{-} macrophages at 8 weeks post-TAC. Importantly, in *late*-treated mice, where IL-1β-mediated-lymphangiogenesis is inhibited, the absence of significant effects on cardiac inflammation, including macrophage levels, suggests generalized dysfunction of the expanded lymphatic network post-TAC. Indeed, we previously showed that the extensive cardiac lymphatic network post-TAC in Balb/c mice is inefficient to resolve cardiac edema, inflammation, and interstitial fibrosis, and thus fails to prevent LV dilation and HF development.[9] Our current study further indirectly demonstrates that *late* anti IL-1β treatment did not suffice to improve cardiac lymphatic drainage post-TAC.

We were surprised by the absence of functional cardiac effects of anti-IL-1β treatment at 8 weeks post-TAC, although *early* anti-IL-1β treatment transiently delayed LV dilation, with beneficial functional effects persisting up to 6 weeks post-TAC. These results contrast with previous studies demonstrating that NLRP3 gene deletion, which reduced IL-1β production, or anti-IL-1β antibody treatment in C57Bl/6J mice, accelerated cardiac dysfunction post-TAC, despite reducing cardiac hypertrophy, macrophage infiltration, and fibrosis.[7,8] It appears that prevention of adaptative hypertrophy, mediated by low levels of IL-1β in C57Bl/6J mice, may promote subsequent development of LV dilation and dysfunction post-TAC, potentially due to increased wall stress. Additionally, the authors suggested insufficient angiogenesis matching cardiac hypertrophy as a driver of accelerated cardiac dysfunction in NLRP3-deficient or anti-IL-1β treated mice[7,8]. In contrast, in Balb/c mice, pressure-overload does not lead to extensive hypertrophy, thus lessening the role of cardiac angiogenesis and the functional impact of potential anti-hypertrophic effects of anti-IL-1β treatment. Indeed, our previous studies have revealed maintenance, but not expansion, of blood vascular networks post-TAC in Balb/c mice.[9] *Of note, Gevokizumab* decreases the binding affinity of IL-1β to IL-1R1, resulting in 30-fold reduction of IL-1β signaling, but it does not completely block IL-1β signaling, different from *Canakinumab* and *Anakinra*.[34] We expect that in our study *early* anti-IL-1β treatment may have reduced, but not completely blocked, cardiac IL-1β signaling, thus maintaining weak but beneficial compensatory hypertrophy[5], while blocking the detrimental direct cardiac effects caused by elevated levels of IL-1β. It is possible that *early* and *prolonged* anti-IL-1β treatment would have been required in our study to reach durable benefit to cardiac function. However, long-term treatment, including during LV dilation, would

have reduced cardiac lymphangiogenesis, thus confounding beneficial direct cardiac effects of IL-1β blockage. Further, the risk for an immune response directed against a therapeutic antibody prevents long-term treatment with *Gevokizumab* in mice.

Other cytokines, including IL-6, may be involved in the pathophysiology of the DCM-like phenotype post-TAC in Balb/c mice. IL-6 has been shown to drive both cardiac fibrosis and pathological hypertrophy following pressure-overload in C57Bl/6 mice.[35] We found that anti-IL-1β treatment did not reduce cardiac *Il6* expression, which may have contributed to the lack of beneficial effects on cardiac fibrosis and HF development found in both *early* and *late* treated-mice. The lack of cardiac benefit of *late* anti-IL-1β treatment suggests that in patients with chronic pressure-overload IL-1β-blocking therapy with may be inefficient, and potentially deleterious, by reducing cardiac lymphatic densities, if initiated during the process of LV dilation. Intriguingly, the beneficial perivascular lymphangiogenesis occurring post-TAC, which appears to protect against perivascular fibrosis, was not influenced by anti-IL-1β treatment. Further studies are needed to identify the triggers of perivascular lymphangiogenesis in the heart and to unravel how these lymphatics prevent perivascular fibrosis during HF development. Notably, a histological marker of edema would be required to investigate if these expanded lymphatics surrounding coronary arterioles suffice to restore locally perivascular pressure-gradients caused by excessive blood vascular leakage during pressure-overload.

Taken together, our study provides, for the first time, a molecular mechanism linking LV dilation to lymphatic remodeling following pressure-overload (**Fig. 5**). Moreover, our data suggests that IL-1β may influence lymphatic expression profiles or secretomes. Intriguingly, the absence of deleterious cardiac effects following inhibition of lymphangiogenesis by *late* anti-IL-1β treatment is in support of our previous suggestion that the expanded lymphatic network in Balb/c mice post-TAC is dysfunctional and/or immature[9]. In contrast, we and other have demonstrated that inhibition of lymphangiogenesis during pressure-overload in C57Bl/6J mice and in Wistar rats, by VEGFR-3 gene deletion or anti-VEGFR-3 treatment, aggravates cardiac inflammation and dysfunction.[9,15,36,37] Further investigations are needed to determine why IL-1β-mediated lymphangiogenesis leads to aberrant hyper-sprouting and dysfunctional cardiac lymphatics in Balb/c mice. Molecular analyses are underway to determine how expanded cardiac lymphatics post-TAC differ from healthy lymphatics in Balb/c mice.

As for the clinical outlook, a recent case-report in a stage III HF patient, secondary to idiopathic inflammatory DCM, demonstrated rapid improvement of LV function following *Anakinra* treatment, associated with reduced IL-6 and BNP levels.[38] We speculate that this cardiac benefit in an already severely dilated heart may be related to positive inotropic effects induced by IL-1β inhibition. In our study, we cannot exclude that the observed inhibition of lymphangiogenesis may have contribute to the lack of functional cardiac benefit of anti-IL-1β in *late*-treated mice. Thus, anti-IL-1β may have a dual therapeutic window where targeting of IL-1β in early stage, before LV dilation, or alternatively at later stage of the disease, where LV dilation and cardiac lymphangiogenesis is well established, may be required to obtain clinical benefit in HF patients.

Material and Methods

Study approval

Animal experiments performed in this study were approved by the regional Normandy ethics review board in line with E.U and French legislation (APAFIS #23175-2019112214599474 v6). A total of 88 Balb/c female mice, surviving TAC or sham-surgery were included in this study. Anonymized human heart samples evaluated in this study were collected with informed consent by the Bichat hospital biobank (*U1148 BB-0033-00029/* BBMRI, coordinator JB Michel) authorized for tissue collection by the Inserm institutional review board as previously reported[9].

Experimental model and reagents

TAC surgery was performed in adult female Balb/c mice (Janvier Laboratories, France). Briefly, a minimally invasive method was used to constrict the aortic arch, using a 26G needle. Double-banding of the aorta was applied to prevent suture internalization and model variability, as described.[9] Anti-IL-1β treatment consisted of a blocking monoclonal antibody against IL-1β, (Gevokizumab/XOMA-052 provided by Servier France), as previously described.[24] The antibody was administered by repeated intraperitoneal injections of 200 µg/mouse (10 mg/kg^{-1}) three times per week starting from week-1 until week-5 post-TAC (*early* treatment) or starting from week-4 until week-8 post-TAC (*late* treatment). Cardiac samples from end-stage HF patients (recipients of cardiac transplants at the Bichat Hospital in Paris, France) were examined by histology. Discarded cardiac autopsy samples, obtained from age-matched donors without cardiovascular disease, were used as healthy controls, as previously reported[9].

Cardiac functional, cellular, and molecular analyses in mice

Cardiac function was evaluated by echocardiography as described.[9] Cardiac sections were analyzed by histology and immunohistochemistry, as described,[9] to determine lymphatic vessel densities and sizes, immune cell infiltration (macrophages), cardiomyocyte hypertrophy, and fibrosis (Sirius Red staining). Perivascular fibrosis was defined as the area of perivascular fibrosis divided by the area of the vascular lumen, averaged over all quantifiable images of arteries taken from a section as described.[28] Cardiac gene expression was analyzed by RT-qPCR. Cardiac protein levels of VEGF-C and VEGF-D were assessed by Western Blot. Cardiac and plasma

levels of IL-1β were evaluated by ELISA (RnD Systems, ELISA DuoSet anti-IL-1β /IL-1F2 #DY401-05). For details see *Suppl. Methods*.

Statistics

Data are presented as mean ± s.e.m. Comparisons were selected to determine: 1) impact of pathology (healthy sham *vs*. TAC); 2) effect of treatment (anti-IL-1β-treated vs. TAC controls). Statistical analyses for comparisons of two independent groups were performed using either Student's two-tailed t-test for groups with normal distribution, or alternatively by Mann Whitney U test for samples where normality could not be ascertained based on D'Agostino & Pearson omnibus normality test. For comparisons of three groups or more either one-way ANOVA followed by Sidak's multiple comparison posthoc (for parameters with n>7 with normal distribution), or alternatively Kruskal-Wallis nonparametric analysis followed by Dunn's posthoc for multiple comparison (for parameters with non-Gaussian distribution) were performed. Longitudinal echocardiography studies were analyzed by paired two-way ANOVA followed by Dunnett's posthoc, while morphometric data and gene expression data were analyzed by two-way ANOVA followed by Sidak's posthoc for multiple pair-wise comparisons or Dunnett's posthoc to compare 3 or more groups. Non-parametric Spearman rank order tests were used for evaluating correlations. Outlier samples were identified as an individual value exceeding group mean±4SD in groups with n≥7. All analyses were performed using GraphPad Prism software.

Author contributions

C.H, O.L and T.L performed and analyzed immunohistochemistry and histology. Echocardiography was performed and analyzed by C.H and T.L ; microgravimetry was carried out by C.H and T.L ; M.V carried out surgical mouse model; C.H carried-out cardiac gene expression analyses, protein analysis by ELISA, and Western Blot; JB.M managed the biobank at Bichat Hospital and contributed clinical data for this study ; P.M and V.T participated in study design; C.H. and E.B designed the study, analyzed results, and prepared the manuscript draft. All authors approved of the final version of the manuscript.

Acknowledgments

We thank Anais Dumesnil, Saida Morchid Azhar, Chloé Valentin, Nousayba Ouattara, and Héloïse Quesnel at Normandy University, Rouen, France for technical assistance with histological analysis, WB, and RTqPCR.

Funding

C.H and T.L were funded by fellowships from the Normandie Doctoral School (EdNBISE). This work was supported by the Fondation pour la Recherche Médicale (FRM) [*FDT202204014960*] to C.H. V.T was funded by the Chair of Excellence program "*Lymphcosign*" from the Normandy Region (RIN Recherche). The research leading to these results benefitted from funding (E.B) from the ERA-CVD Research Programme, which is a transnational R&D programme jointly funded by national funding organisations [*ANR-16-ECVD-0004*] within the framework of the ERA-NET ERA-CVD. This work was further supported by a grant from the GCS G4 and the Normandy region (FHU CARNAVAL) and by a grant (E.B) from the Agence Nationale de la Recherche (ANR) for the project "CITE-LYMPH" [*ANR-22-CE92-0040*]. The project also benefitted from generalized institutional funds (Inserm U1096 laboratory) from French Inserm and the Normandy Region together with the European Union: "*Europe gets involved in Normandie*" with European Regional Development Fund (ERDF): CPER/FEDER 2015 [DO-IT] and CPER/FEDER 2016 [PACT-CBS].

Conflict of Interest

The authors declare that they have no conflict of interest.

References

1. Ridker, P. M. *et al.* Antiinflammatory Therapy with Canakinumab for Atherosclerotic Disease. *N Engl J Med* **377**, 1119–1131 (2017).
2. Abbate, A. *et al.* Interleukin-1 and the Inflammasome as Therapeutic Targets in Cardiovascular Disease. *Circ Res* **126**, 1260–1280 (2020).
3. Zeng, C. *et al.* NLRP3 inflammasome-mediated pyroptosis contributes to the pathogenesis of non-ischemic dilated cardiomyopathy. *Redox Biol* **34**, 101523 (2020).
4. Li, H., Chen, C. & Wang, D. W. Inflammatory Cytokines, Immune Cells, and Organ Interactions in Heart Failure. *Front Physiol* **12**, 695047 (2021).
5. Honsho, S. *et al.* Pressure-mediated hypertrophy and mechanical stretch induces IL-1 release and subsequent IGF-1 generation to maintain compensative hypertrophy by affecting Akt and JNK pathways. *Circ Res* **105**, 1149–1158 (2009).
6. Sano, S. *et al.* Tet2-Mediated Clonal Hematopoiesis Accelerates Heart Failure Through a Mechanism Involving the IL-1β/NLRP3 Inflammasome. *J Am Coll Cardiol* **71**, 875–886 (2018).
7. Higashikuni, Y. *et al.* Toll-like receptor-2 mediates adaptive cardiac hypertrophy in response to pressure overload through interleukin-1β upregulation via nuclear factor κB activation. *J Am Heart Assoc* **2**, e000267 (2013).
8. Higashikuni, Y. *et al.* NLRP3 Inflammasome Activation Through Heart-Brain Interaction Initiates Cardiac Inflammation and Hypertrophy During Pressure Overload. *Circulation* (2022) doi:10.1161/CIRCULATIONAHA.122.060860.
9. Heron, C. *et al.* Regulation and impact of cardiac lymphangiogenesis in pressure-overload-induced heart failure. *Cardiovasc Res* cvac086 (2022) doi:10.1093/cvr/cvac086.
10. Henri, O. *et al.* Selective Stimulation of Cardiac Lymphangiogenesis Reduces Myocardial Edema and Fibrosis Leading to Improved Cardiac Function Following Myocardial Infarction. *Circulation* **133**, 1484–1497; discussion 1497 (2016).
11. Vieira, J. M. *et al.* The cardiac lymphatic system stimulates resolution of inflammation following myocardial infarction. *J Clin Invest* **128**, 3402–3412 (2018).
12. Houssari, M. *et al.* Lymphatic and Immune Cell Cross-Talk Regulates Cardiac Recovery After Experimental Myocardial Infarction. *Arterioscler Thromb Vasc Biol* **40**, 1722–1737 (2020).
13. Trincot, C. E. *et al.* Adrenomedullin Induces Cardiac Lymphangiogenesis After Myocardial Infarction and Regulates Cardiac Edema Via Connexin 43. *Circ Res* **124**, 101–113 (2019).
14. Song, L. *et al.* Lymphangiogenic therapy prevents cardiac dysfunction by ameliorating inflammation and hypertension. *Elife* **9**, e58376 (2020).
15. Yang, G.-H. *et al.* Overexpression of VEGF-C attenuates chronic high salt intake-induced left ventricular maladaptive remodeling in spontaneously hypertensive rats. *Am J Physiol Heart Circ Physiol* **306**, H598-609 (2014).
16. Weichand, B. *et al.* S1PR1 on tumor-associated macrophages promotes lymphangiogenesis and metastasis via NLRP3/IL-1β. *J Exp Med* **214**, 2695–2713 (2017).
17. Watari, K. *et al.* Role of macrophages in inflammatory lymphangiogenesis: Enhanced production of vascular endothelial growth factor C and D through NF-kappaB activation. *Biochem Biophys Res Commun* **377**, 826–831 (2008).

18. Sáinz-Jaspeado, M. & Claesson-Welsh, L. Cytokines regulating lymphangiogenesis. *Curr Opin Immunol* **53**, 58–63 (2018).
19. Baluk, P. *et al.* Transgenic overexpression of interleukin-1β induces persistent lymphangiogenesis but not angiogenesis in mouse airways. *Am J Pathol* **182**, 1434–1447 (2013).
20. Scallan, J. P., Zawieja, S. D., Castorena-Gonzalez, J. A. & Davis, M. J. Lymphatic pumping: mechanics, mechanisms and malfunction. *J Physiol* **594**, 5749–5768 (2016).
21. Brakenhielm, E., González, A. & Díez, J. Role of Cardiac Lymphatics in Myocardial Edema and Fibrosis: JACC Review Topic of the Week. *J Am Coll Cardiol* **76**, 735–744 (2020).
22. Kleiner, J. L. *et al.* Characterization of Transverse Aortic Constriction in Mice Based on the Specific Recruitment of Leukocytes to the Hypertrophic Myocardium and the Aorta Ascendens. *Mediators Inflamm* **2021**, 1376859 (2021).
23. Patel, B., Ismahil, M. A., Hamid, T., Bansal, S. S. & Prabhu, S. D. Mononuclear Phagocytes Are Dispensable for Cardiac Remodeling in Established Pressure-Overload Heart Failure. *PLoS One* **12**, e0170781 (2017).
24. Harouki, N. *et al.* The IL-1β Antibody Gevokizumab Limits Cardiac Remodeling and Coronary Dysfunction in Rats With Heart Failure. *JACC Basic Transl Sci* **2**, 418–430 (2017).
25. Bizou, M. *et al.* Cardiac macrophage subsets differentially regulate lymphatic network remodeling during pressure overload. *Sci Rep* **11**, 16801 (2021).
26. Künnapuu, J., Bokharaie, H. & Jeltsch, M. Proteolytic Cleavages in the VEGF Family: Generating Diversity among Angiogenic VEGFs, Essential for the Activation of Lymphangiogenic VEGFs. *Biology (Basel)* **10**, 167 (2021).
27. Loef, E. J., Sheppard, H. M., Birch, N. P. & Dunbar, P. R. Plasminogen and plasmin can bind to human T cells and generate truncated CCL21 that increases dendritic cell chemotactic responses. *J Biol Chem* **298**, 102112 (2022).
28. Dai, Z., Aoki, T., Fukumoto, Y. & Shimokawa, H. Coronary perivascular fibrosis is associated with impairment of coronary blood flow in patients with non-ischemic heart failure. *J Cardiol* **60**, 416–421 (2012).
29. Zhu, G. *et al.* Lipopolysaccharide increases the release of VEGF-C that enhances cell motility and promotes lymphangiogenesis and lymphatic metastasis through the TLR4-NF-κB/JNK pathways in colorectal cancer. *Oncotarget* **7**, 73711–73724 (2016).
30. Boermeester, M. A. *et al.* Interleukin-1 blockade attenuates mediator release and dysregulation of the hemostatic mechanism during human sepsis. *Arch Surg* **130**, 739–748 (1995).
31. Tal, O. *et al.* DC mobilization from the skin requires docking to immobilized CCL21 on lymphatic endothelium and intralymphatic crawling. *J Exp Med* **208**, 2141–2153 (2011).
32. Bromley, S. K., Thomas, S. Y. & Luster, A. D. Chemokine receptor CCR7 guides T cell exit from peripheral tissues and entry into afferent lymphatics. *Nat Immunol* **6**, 895–901 (2005).
33. Martini, E. *et al.* Single-Cell Sequencing of Mouse Heart Immune Infiltrate in Pressure Overload-Driven Heart Failure Reveals Extent of Immune Activation. *Circulation* **140**, 2089–2107 (2019).
34. Issafras, H., Corbin, J. A., Goldfine, I. D. & Roell, M. K. Detailed mechanistic analysis of gevokizumab, an allosteric anti-IL-1β antibody with differential receptor-modulating properties. *J Pharmacol Exp Ther* **348**, 202–215 (2014).

35. Lai, N. C. *et al.* Pressure overload-induced cardiac remodeling and dysfunction in the absence of interleukin 6 in mice. *Lab Invest* **92**, 1518–1526 (2012).
36. Lin, Q.-Y., Zhang, Y.-L., Bai, J., Liu, J.-Q. & Li, H.-H. VEGF-C/VEGFR-3 axis protects against pressure-overload induced cardiac dysfunction through regulation of lymphangiogenesis. *Clin Transl Med* **11**, e374 (2021).
37. Bai, J. *et al.* Angiotensin II Induces Cardiac Edema and Hypertrophic Remodeling through Lymphatic-Dependent Mechanisms. *Oxid Med Cell Longev* **2022**, 5044046 (2022).
38. De Luca, G., Campochiaro, C., Dinarello, C. A., Dagna, L. & Cavalli, G. Treatment of Dilated Cardiomyopathy With Interleukin-1 Inhibition. *Ann Intern Med* **169**, 819–820 (2018).

Figures & Legends

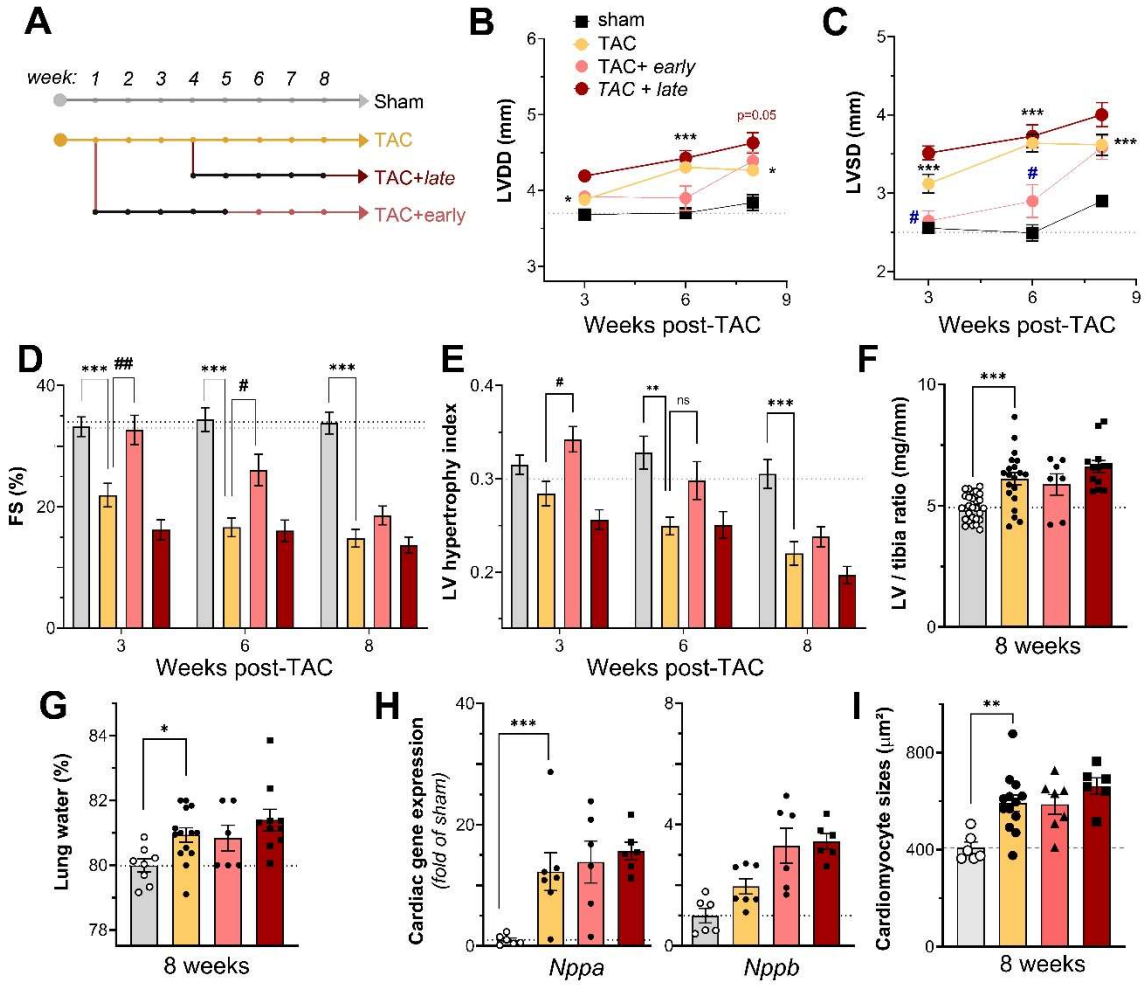

Figure 1 Early anti-IL-1β treatment transiently delays LV dilation but does not impact HF development at 8 weeks post-TAC in Balb/c mice

Schematic overview of the study (**a**). Echocardiography at 3, 6 and 8 weeks post-TAC in sham (*n=29;* grey bars w. white circles), control TAC (*n=18;* yellow bars w. black circles), and *early* (*n=8;* red bars w. black circles) vs. *late* (n=*10;* red bars w. black squares) anti-IL-1β-treated TAC mice was used to assess LV diastolic diameter (*LVDD*, **b**) and LV systolic diameter (*LVSD*, **c**), and to calculate fractional shortening (*FS*, **d**). LV hypertrophy dilatation index (**e**) Morphometric assessment of left ventricular (LV) weights normalized to tibia lengths at 8 weeks (**f**), and lung water content (**g**). Cardiac expression analyses at 8 weeks of *Nppa* and *Nppb* (**h**, *n= 6-7* per group). Analysis and examples of cardiomyocyte cross-sectional area (**i**, *n=6-13* animals per group) at 8 weeks. Groups were compared by two-way ANOVA followed by Dunnett's multiple comparison test (panels **b-e, i**), by one-way ANOVA followed by Sidak's multiple comparison test (**g, h**), or by non-parametric Kruskal Wallis followed by Dunn's posthoc test (**i**) * p<0.05, ** p<0.01, *** p<0.001 *versus* sham; # p<0.05; ## p<0.01 *versus* TAC control.

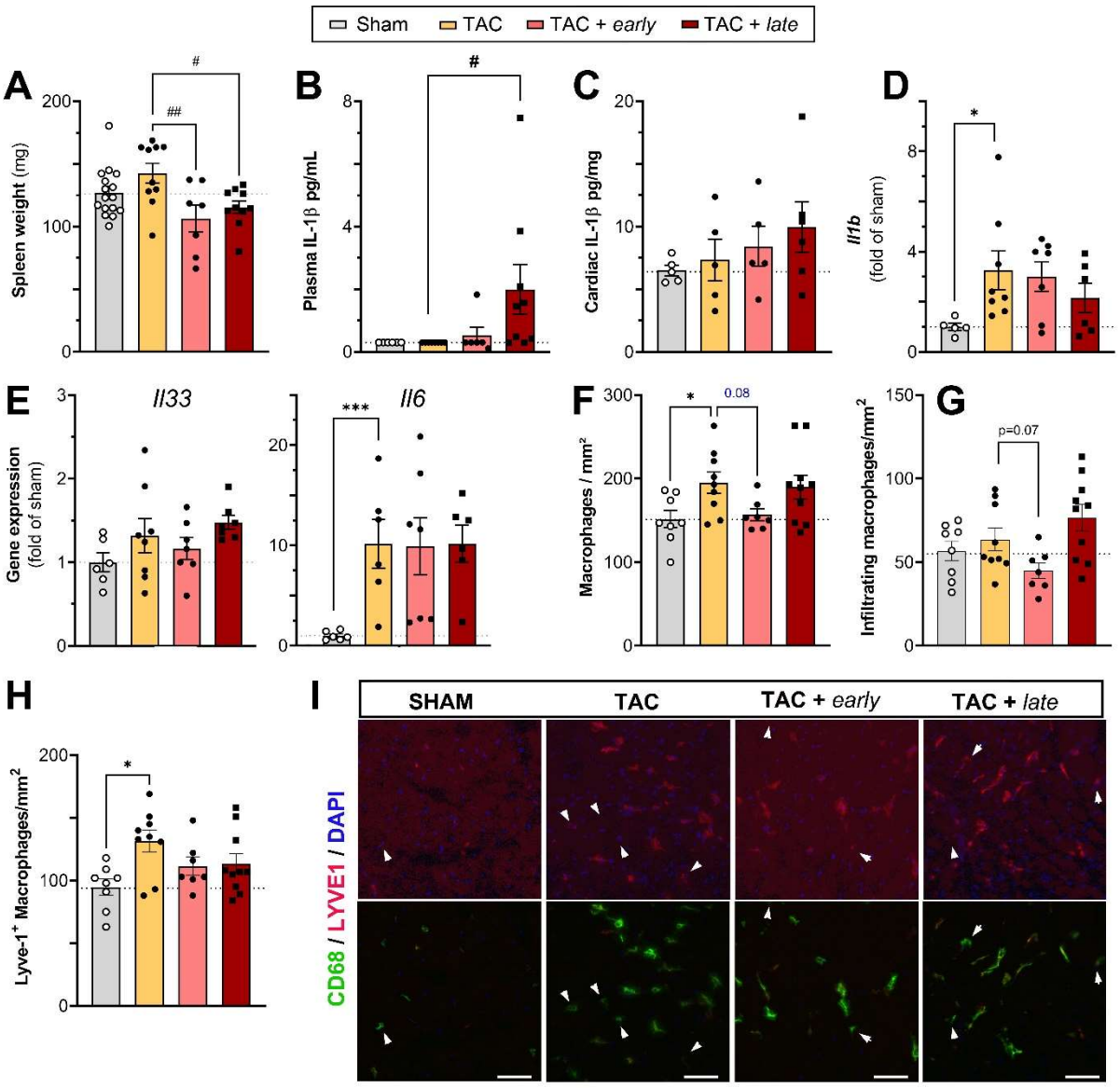

Figure 2 Anti-IL-1β treatment has weak impact on cardiac inflammation post-TAC

Morphometric assessment of spleen weights at 8 weeks (**a**) in sham (*n=16;* grey bars w. white circles), control TAC (*n=10;* yellow bars w. black circles), and *early* (*n=7;* red bars w. black circles) vs. *late* (n=*10;* red bars w. black squares) anti-IL-1β-treated TAC mice. Plasma (**b**) and cardiac (**c**) IL-1β protein levels evaluated by ELISA at 8 weeks post-TAC (*n=5-10* mice per group). Cardiac *Il1b* (**d**), and *Il33* and *Il6* gene expression (**e**) evaluated by qPCR at 8 weeks post-TAC (*n=5-8* mice per group). Quantification of total cardiac CD68$^+$ macrophage levels evaluated by immunohistochemistry at 8 weeks (**f**). Quantification of infiltrating CD68$^+$Lyve1$^-$ macrophages (**g**) and residential CD68$^+$ / Lyve1$^+$ macrophages (**h**) (*n=7-10* mice per group). Examples of cardiac macrophages (**i**). CD68, *green*, Lyve1, *red*, Dapi *blue*, Scalebar 50 µm. Arrowheads point to infiltrating CD68$^+$/Lyve1$^-$ macrophages. Groups were compared by one-way ANOVA followed by Sidak's multiple comparison test (**a, c**), by non-parametric Kruskal Wallis followed by Dunn's multiple comparison posthoc test (**b, e, g, h**), or by mixed-effect analysis followed by Sidak's multiple comparison test (**d**). * p<0.05, *** p<0.001 *versus* sham; # p<0.05; ## p<0.01 *versus* TAC control.

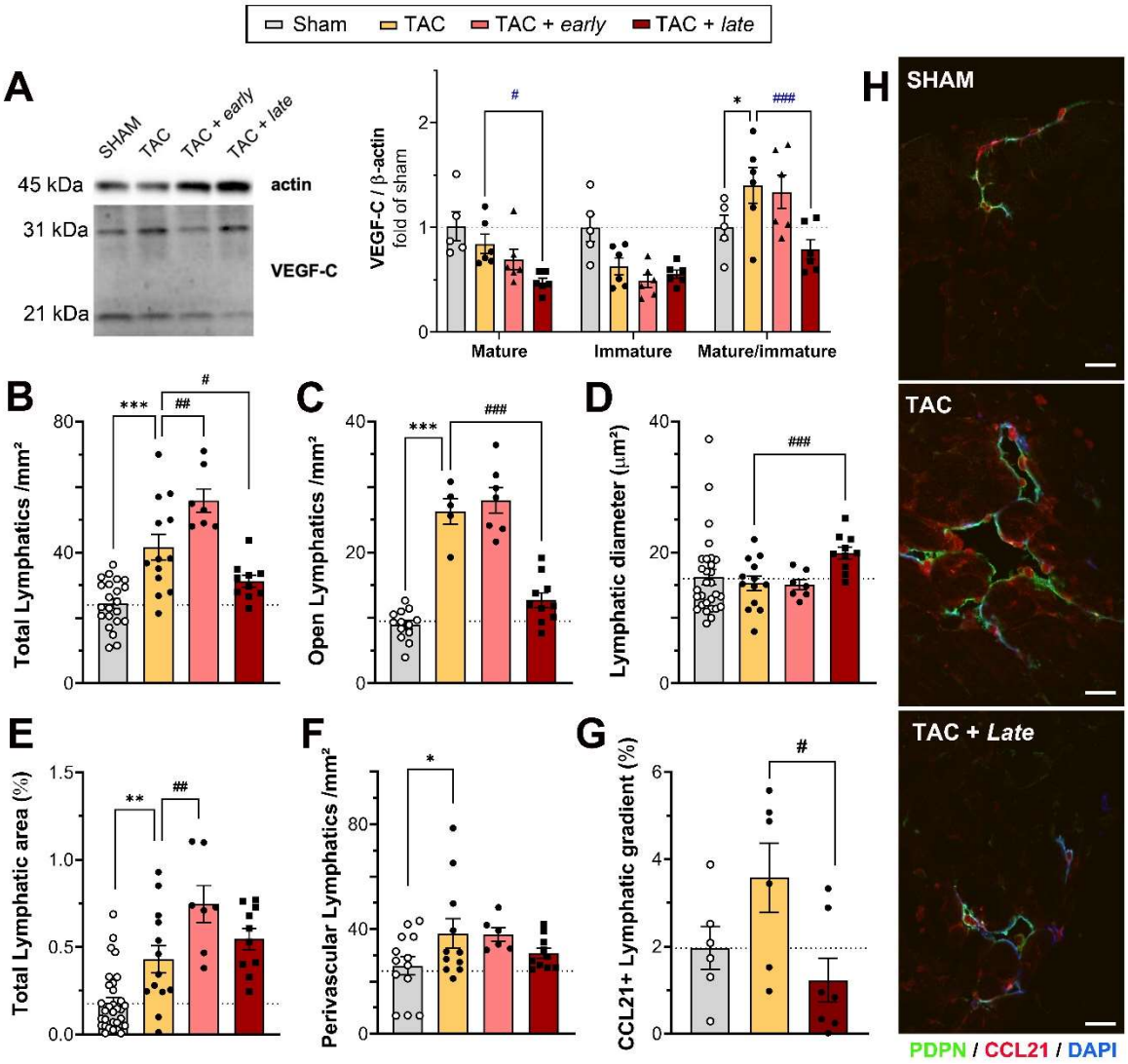

Figure 3 *Late* anti-IL-1β treatment reduces TAC-induced cardiac lymphangiogenesis

Examples and quantification (**a**) of VEGF-C protein levels (21 kDa mature vs 31 kDa immature monomeric isoforms) in cardiac samples at 8 weeks post-TAC in sham (*n=5;* grey bars w. white circles), control TAC (*n=5;* yellow bars w. black circles), and *early* (*n=5;* red bars w. black circles) vs. *late* (n=*5;* red bars w. black squares) anti-IL-1β-treated TAC mice. Cardiac capillary lymphatic density (**b**), open vessel density (**c**), lymphatic vessel lumen sizes (**d**), lymphatic vascular area (**e**), and perivascular lymphatic density (**f**) were evaluated in histological sections at 8 weeks post-TAC (*n= 6-13* mice per group). Quantification of CCL21 gradients in cardiac lymphatics (**g**). Examples of cardiac lymphatic chemokine gradients (**h**): Podoplanin (PDPN), *green*; CCL21, *red*, Dapi *blue*. Scalebar 50 µm. Groups were compared by non-parametric Kruskal Wallis followed by Dunn's posthoc test (**b, c, d, e, f, g**) or by two-way ANOVA followed by Dunnett's multiple comparisons test (**a**). * p<0.05 *versus* sham, ## p<0.01, ### p<0.001 *versus* TAC control.

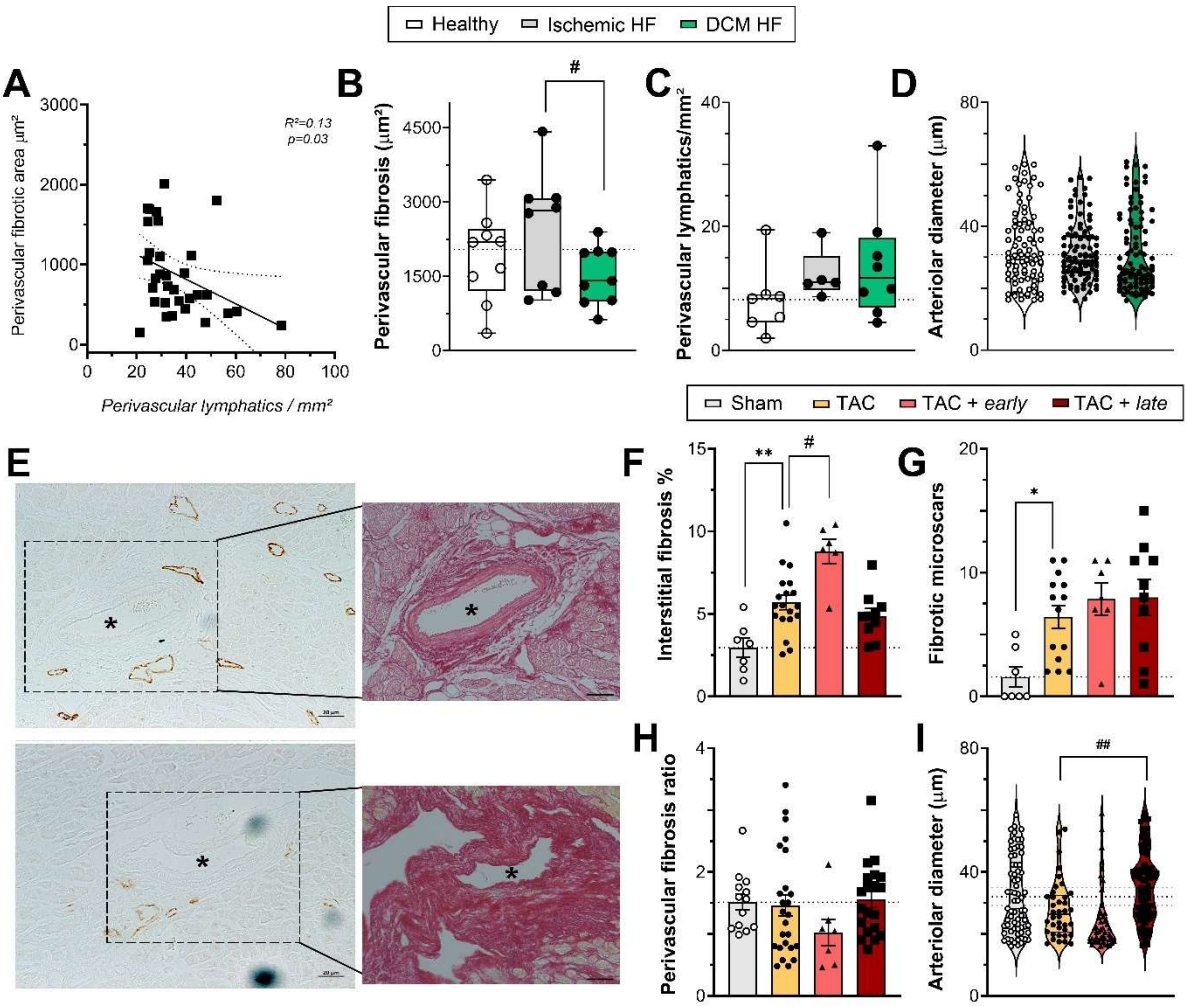

Figure 4 Cardiac perivascular fibrosis post-TAC in mice and HF patients linked to perivascular lymphatics, independently of IL-1β

Correlation analysis of perivascular fibrosis, calculated as the ratio of fibrotic area normalized to blood vessel lumen area in arterioles, and cardiac lymphatic capillary density in mice at 8 weeks post-TAC (**a**). Quantification of perivascular fibrosis areas in healthy controls (*n=9*, white bar), ischemic HF patients (*n=8, grey bar*), and DCM patients (*n=9, green bar*) (**B**). Arteriolar sizes used for evaluation of perivascular fibrosis in patients (**c**). Quantification of perivascular lymphatic densities in patients (**d**, adapted from Heron *et al.*[9]). Examples (**e**) of cardiac perivascular lymphatics, stained for PDPN, and perivascular fibrosis in Sirius Red-stained clinical HF samples; scalebar 20 µm. Evaluation of interstitial fibrosis (**f**) at 8 weeks post-TAC in sham (*n=7;* grey bars w. white circles), control TAC (*n=19;* yellow bars w. black circles), and *early* (*n=6;* red bars w. black circles) vs. *late* (n=*10;* red bars w. black squares) anti-IL-1β-treated TAC mice. Quantification of microscars (**g**) and perivascular fibrosis ratios (**h**) at 8 weeks post-TAC. Arteriolar lumen size profiles (**i**) for analysis of perivascular fibrosis. Groups were compared by one-way ANOVA followed by Sidak's multiple comparison test (**c, i**) or by non-parametric Kruskal Wallis followed by Dunn's posthoc test (**b, d, f, g, h**). * p<0.05 *versus* sham, ## p<0.01, ### p<0.001 *versus* TAC control or DCM patients. Non-parametric Spearman rank order test was used for correlation (**a**).

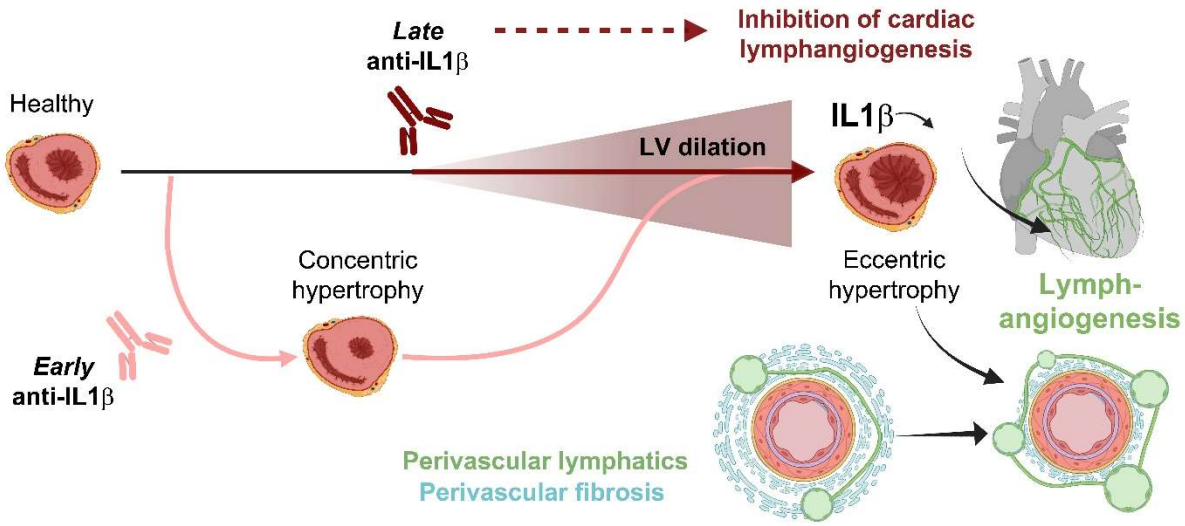

Figure 5 Schematic view of cardiac impact of IL-1β during pressure-overload

LV dilation increases cardiac IL-1β levels, stimulating VEGF-C-dependent cardiac lymphangiogenesis and increased lymphatic CCL21 gradients. However, in the setting of cardiac inflammation, the expanded lymphatic network remains immature and/or dysfunctional, and fails to limit accumulation of immune cells, edema, and interstitial fibrosis. In contrast, perivascular lymphangiogenesis, triggered in an IL-1β-independent manner during LV dilation, suffices to limit perivascular fibrosis following pressure-overload. Further, we demonstrate that antibody-mediated blockage of IL-1β in *early* phase post-TAC in Balb/c mice, before onset of lymphangiogenesis, transiently limits LV dilation. In contrast, *late* treatment, initiated during LV dilation, blocks cardiac lymphangiogenesis, but not perivascular lymphangiogenesis, and does not improve cardiac remodelling or dysfunction.

Table 1 – Echocardiography at 8 weeks post-TAC in Balb/c mice

parameter		Sham		TAC	TAC + *early*		TAC + *late*	
n		*8*	*p*	*26*	*7*	*p*	*10*	*p*
BW	*g*	**26**±0.4	*ns*	**25**±0.4	**23**±1.2	*ns*	**26**±0.5	*ns*
HR	*bpm*	**338**±8	*ns*	**368**±11	**380**±20	*ns*	**345**±12	*ns*
AWT ED	*mm*	**0.7**±0.05	*ns*	**0.8**±0.02	**0.8**±0.06	*ns*	**0.8**±0.03	*ns*
AWT ES	*mm*	**0.9**±0.04	*	**1.0**±0.03	**1.1**±0.04	*ns*	**0.9**±0.04	*ns*
PWT ED	*mm*	**0.7**±0.03	*ns*	**0.8**±0.03	**0.8**±0.05	*ns*	**0.8**±0.03	*ns*
PWT ES	*mm*	**0.9**±0.03	*ns*	**1.0**±0.04	**1.0**±0.07	*ns*	**0.9**±0.02	*ns*
LVDD	*mm*	**3.8**±0.1	*	**4.3**±0.06	**4.4**±0.1	*ns*	**4.6**±0.1	*ns*
LVSD	*mm*	**2.9**±0.1	***	**3.6**±0.1	**3.6**±0.2	*ns*	**4.0**±0.2	*ns*
FS	*%*	**24**±1.8	*	**17**±1.1	**19**±2	*ns*	**14**±1	*ns*
VTI	*cm*	**2.3**±0.3	*ns*	**1.8**±0.09	**2.4**±0.2	*ns*	**1.7**±0.2	*ns*
SV	*µL*	**58**±6	*ns*	**46**±3	**64**±7	*ns*	**50**±6	*ns*
CO	*µL/min*	**19**±2	*ns*	**17**±1	**24**±3	*ns*	**17**±2	*ns*
EDV	*µL*	**64**±4	*ns*	**72**±5	**55**±6	*ns*	**100**±3	**
ESV	*µL*	**32**±2	***	**62**±4	**88**±5	**	**72**±6	*ns*
EF	*%*	**49**±3	**	**35**±2	**38**±3	*ns*	**29**±3	*ns*

BW, body weight; *HR*, heart rate; *AWT ED*, anterior wall thickness end-diastole; *AWT ES*, anterior wall thickness end-systole; *PWT ED*, posterior wall thickness end-diastole; *PWT ES*, posterior wall thickness end-systole; *LVDD*, left ventricular diastolic diameter; LVSD, left ventricular systolic diameter; *FS*, fractional shortening: *VTI*, velocity time integral; *SV*, stroke volume; *CO*, cardiac output; *EDV*, end diastolic volume; *ESV* end systolic volume; *EF*, ejection fraction. All samples were compared using Two-way ANOVA followed by Sidak's posthoc test. * p<0.05; ** p<0,001; *** p<0.001 *versus* TAC controls.

Supplementary methods & materials

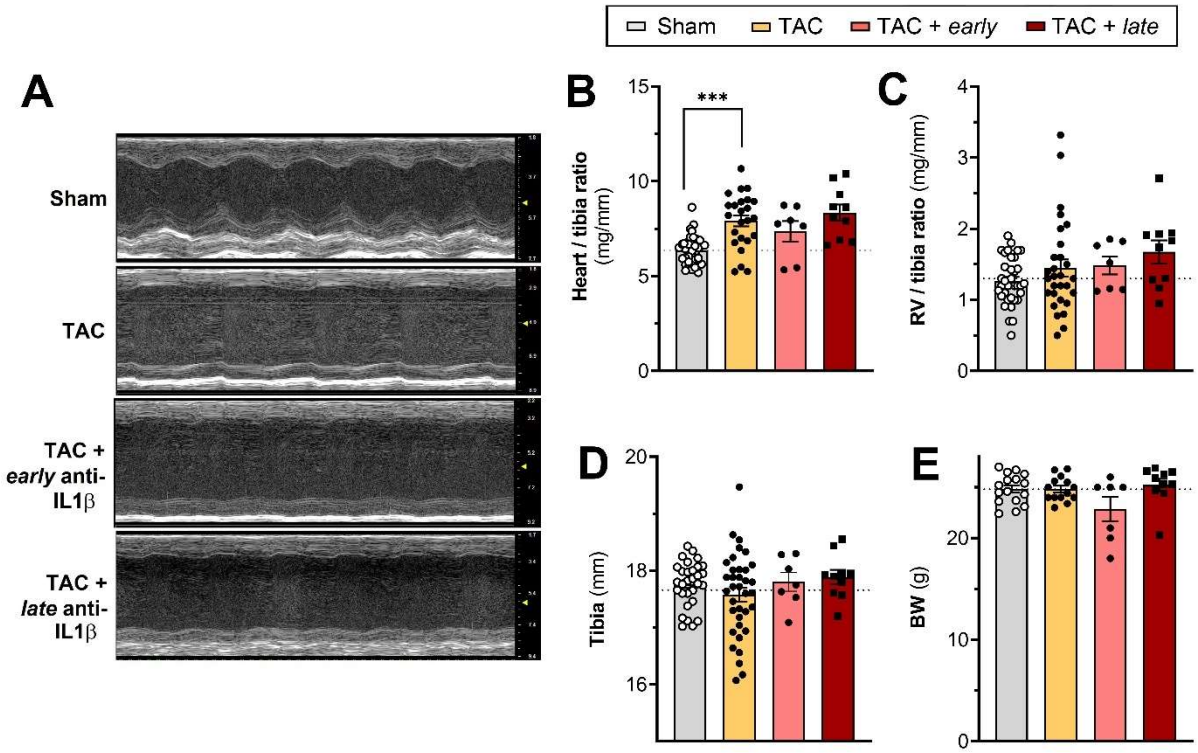

Suppl. Fig. 1- Morphometric analyses at 8 weeks post-TAC

Examples of echocardiography short-axis views (**a**). Assessment of cardiac (**b**) and right ventricular (RV) weights (**c**), normalized to tibia lengths (**d**), and body weight (**e**) at 8 weeks in sham (*n=16-30;* grey bars w. white circles), control TAC (*n=10-36;* yellow bars w. black circles), and *early* (*n=7;* red bars w. black circles) vs. *late* (n=*10;* red bars w. black squares) anti-IL-1β-treated TAC mice. Groups were compared by one-way ANOVA followed by Sidak's multiple comparison test * p<0.05 *versus* sham, ## p<0.01, ### p<0.001 *versus* TAC control.

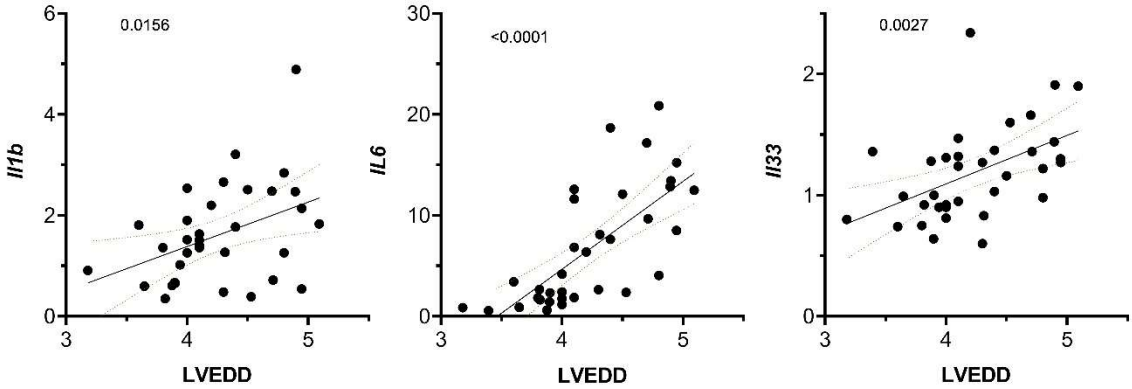

Suppl. Fig. 2 -Correlation between LV EDD and cardiac cytokine expression

Evaluation of the degree of LV dilation (LV EDD) and cardiac gene expression levels (*fold of sham*) of *Il1b* (**a**), *Il6* (**b**), and *Il33* (**c**) at 8 weeks post-TAC in Balb/c mice. Non-parametric Spearman rank order tests were used for evaluating correlations.

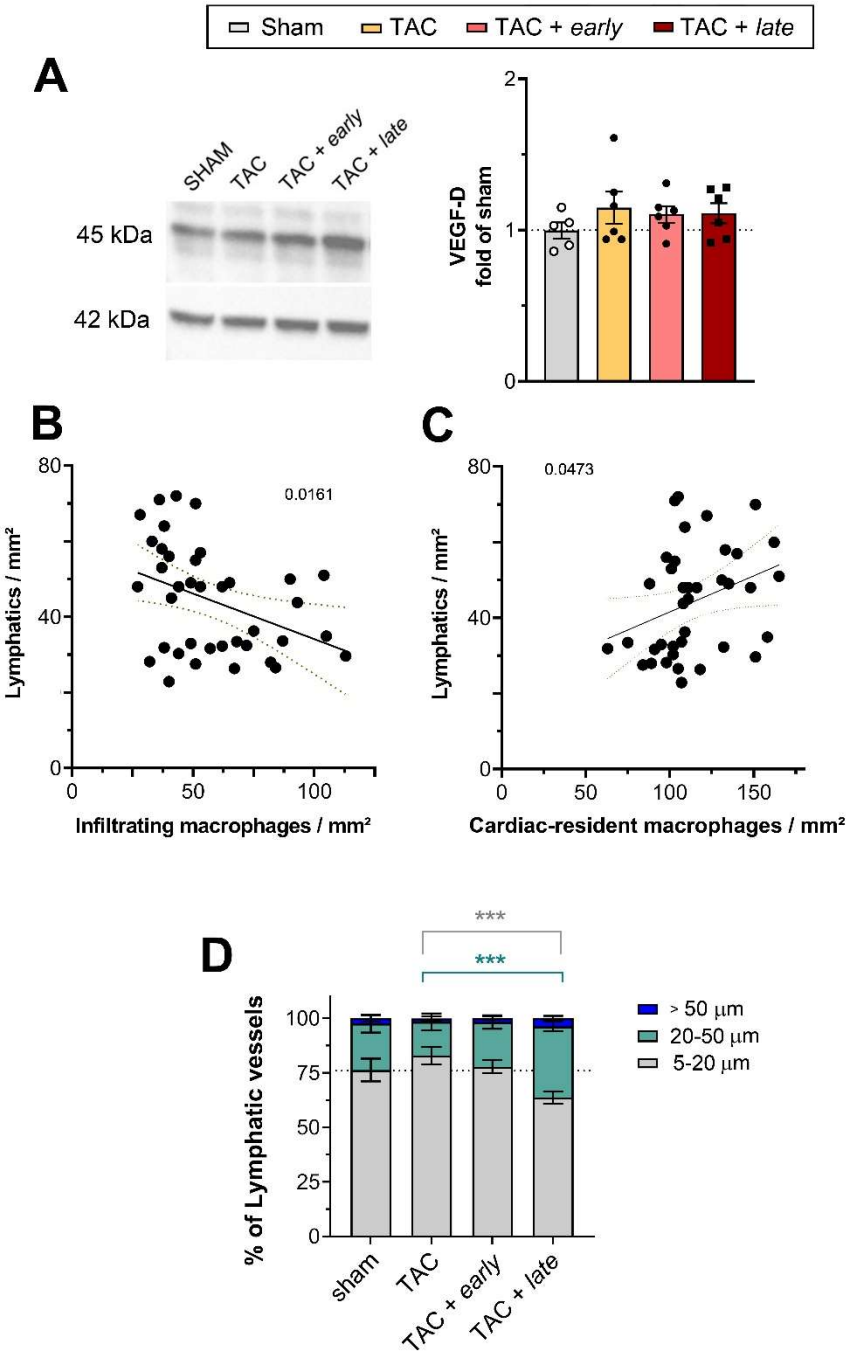

Suppl. Fig. 3 -Cardiac VEGF-D levels and vessel size profiles post-TAC

Western blot analysis of cardiac samples at 8 weeks of VEGF-D protein levels in sham (*n=5;* grey bars w. white circles), control TAC (*n=5;* yellow bars w. black circles), and *early* (*n=5;* red bars w. black circles) vs. *late* (n=*5;* red bars w. black squares) anti-IL-1β-treated TAC mice (**a**). Correlation between cardiac-infiltrating macrophages (**b**) or resident CD68$^+$ LYVE1$^+$ macrophages (**c**) versus lymphatic densities post-TAC. Evaluation of lymphatic lumen size profiles at 8 weeks post-TAC (**d**) (on average 39 vessels analyzed/mouse: *n=10* mouse/group).

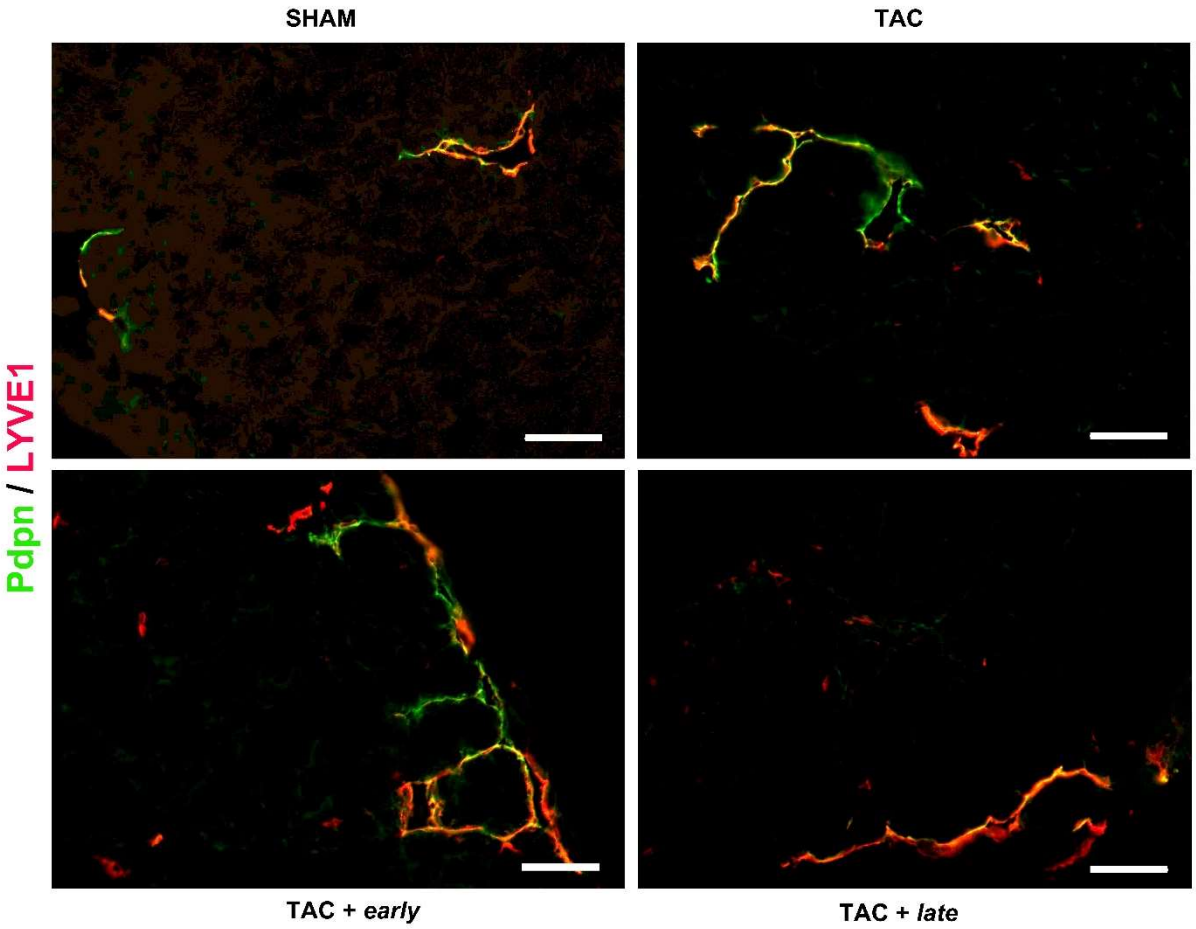

Suppl. Fig. 4 -Cardiac lymphatic network post-TAC

Evaluation of lymphatic vessel densities at 8 weeks post-TAC using a combination of LYVE1 (*red*) and Podoplanin (Pdpn, *green*) in cardiac sections. Scalebar 50 µm.

Suppl. Table 1 – Cardiac function evaluated by echocardiography at 6-weeks post-TAC

parameter		Sham		TAC	TAC + *early*		TAC + *late*	
n		*26*	*p*	*33*	*7*	*p*	*10*	*p*
HR	*bpm*	**355**±9	*n.s*	**382**±9	**443**±31	*n.s*	**391**±14	*n.s*
AWT ED	*mm*	**0.8**±0.03	**	**0.9**±0.02	**0.8**±0.07	*n.s*	**0.9**±0.03	*n.s*
AWT ES	*mm*	**1.2**±0.05	*n.s*	**1.2**±0.04	**1.21**±0.1	*n.s*	**1.2**±0.05	*n.s*
PWT ED	*mm*	**0.8**±0.04	*n.s*	**0.9**±0.03	**0.8**±0.04	*n.s*	**0.8**±0.04	*n.s*
PWT ES	*mm*	**1.1**±0.06	*n.s*	**1.1**±0.03	**1.1**±0.04	*n.s*	**1.0**±0.05	*n.s*
LVDD	*mm*	**3.7**±0.06	***	**4.3**±0.06	**3.9**±0.2	*n.s*	**4.4**±0.1	*n.s*
LVSD	*mm*	**2.5**±0.1	***	**3.6**±0.08	**2.9**±0.2	*	**3.7**±0.1	*n.s*
FS	*%*	**33**±2	***	**18**±1.1	**26**±3	*	**16**±1.8	*n.s*
VTI	*cm*	**1.9**±0.1	*n.s*	**2.0**±0.2	**2.3**±0.1	*n.s*	**1.8**±0.1	*n.s*
SV	*µL*	**56**±3	*n.s*	**60**±7	**59**±5	*n.s*	**47**±5	*n.s*
CO	*µL/min*	**20**±1	*n.s*	**23**±3	**26**±3	*n.s*	**18**±2	*n.s*
EDV	*µL*	**60**±3	***	**77**±4	**35**±6	***	**89**±4	*n.s*
ESV	*µL*	**24**±2	***	**60**±4	**67**±7	*n.s*	**61**±5	*n.s*
EF	*%*	**62**±3	***	**39**±2	**51**±4	*n.s*	**34**±3	*n.s*

BW, body weight; *HR*, heart rate; *AWT ED*, anterior wall thickness end-diastole; *AWT ES*, anterior wall thickness end-systole; *PWT ED*, posterior wall thickness end-diastole; *PWT ES*, posterior wall thickness end-systole; *LVDD*, left ventricular diastolic diameter; LVSD, left ventricular systolic diameter; *FS*, fractional shortening: *VTI*, velocity time integral; *SV*, stroke volume; *CO*, cardiac output; *EDV*, end diastolic volume; *ESV* end systolic volume; *EF*, ejection fraction. All samples were compared using Two-way ANOVA followed by Sidak's posthoc test. * p<0.05; ** p<0,001; *** p<0.001 *versus* TAC controls.

Suppl. Table 2 – Cardiac gene expression at 8 weeks post-TAC

	Sham		TAC	TAC + *early*		TAC + *late*	
gene	*6*	*p*	*8*	*7*	*p*	*7*	*p*
Lyve1	**1.00**±0.05	*n.s*	**1.14**±0.18	**1.41**±0.17	*n.s*	**2.20**±0.17	***
Pdpn	**1.00**±0.11	***	**2.21**±0.28	**2.25**±0.35	*n.s*	**2.12**±0.09	*n.s*
Ccl21	**1.00**±0.09	*n.s*	**1.21**±0.14	**1.44**±0.23	*n.s*	**1.91**±0.13	*
Vegfc	**1.00**±0.06	*	**1.65**±0.13	**1.82**±0.18	*n.s*	**1.71**±0.08	*n.s*
Vegfd	**1.00**±0.09	*n.s*	**1.48**±0.3	**1.12**±0.08	*n.s*	**0.88**±0.08	*

All samples were compared using Two-way ANOVA followed by Sidak's posthoc test. * p<0.05; ** p<0,001; *** p<0.001 *versus* TAC controls.

Suppl. Methods & Materials

Human samples

Five micrometer thick sections were prepared from paraffin-embedded human septal samples. Standard immunohistological protocols, including citrate antigen retrieval, were used to reveal podoplanin-positive lymphatic vessels using a mouse anti-human podoplanin/D2-40 antibody validated for clinical practice (Dako, # M3619, diluted *1:50*). Signal was revealed following incubation with HRP-conjugated donkey anti-mouse secondary, followed by DAB detection kit (Vector Laboratories, Burlingame, CA). All patient slides were processed together for uniformity. Lymphatics were examined using a Zeiss axiovision light microscope equipped with CCD cameras at *x10.* Lymphatic vessels, identified as Podoplanin$^+$ vascular structures in the subendocardium, were counted by an observer blinded to the patient category. Total lymphatic density, open lymphatic density (lumenized vessels), lymphatic vessel diameter, and density of perivascular lymphatics (defined as lymphatics within 200 µm distance of a large blood vessel) were determined. On average for each patient 1.2 ±0.2 mm² of the septal sample was analyzed to determine lymphatic vessel sizes and densities.

Experimental Model

Female Balb/c mice (22-24 g) were obtained from Janvier. Animal housing and experiments were in accordance with National Institutes of Health guidelines, and the study was ethically approved by the Normandy University regional review board according to French and EU legislation (APAFIS #**23175**-2019112214599474 v6; APAFIS #**32433**-2022070712508369 v2). Minimally-invasive transversal aortic banding constriction (TAC) was performed on 8 week-old mice, as previously described.[1] Mice were anaesthetized by intraperitoneal injection of ketamine (100 mg kg $^{-1}$ Imalgene®) and xylazine (10 mg kg $^{-1}$ Rompun® 2%, Bayer Health Care) and placed on mechanical ventilation. The operator performed a minimal thoracotomy with an incision at the level of the first intercostal space. The aortic arch was visualized under low-power magnification. A snare, made of 7-0 polypropylene suture, was passed under the aorta between the origin of the right innominate and left common carotid arteries. Two suture bands were placed side-by-side to create an elongated stenosis and prevent internalization of the suture, as described.[2] A bent 26-gauge needle was placed next to the aortic arch, and the sutures were snugly tied around the needle and the aorta. After banding, the needle was quickly removed. The skin was closed, and mice recovered on a warming pad until fully awake. The sham procedure was identical except that the aorta was not banded. Buprenorphine (50 µg/kg, Buprecare®, Axcience) was injected subcutaneously 6 hours after surgery and twice per day until 3 days post-operation. Anti-IL-1β treatment consisted of a blocking monoclonal antibody against IL-1β, (Gevokizumab/XOMA-052 provided by Servier France), as previously described.[3] The antibody was administered by repeated intraperitoneal injections of 200 µg/mouse (10 mg/kg^{-1}) three times per week starting from week-1 until week-5 post-TAC (*early* treatment) or starting from week-4 until week-8 post-TAC (*late* treatment).

Echocardiography

Transthoracic echocardiography measurements (Doppler and M-mode) were performed in animals anaesthetized with isoflurane (1-2%), using a Vevo 3100 Imaging System (FUJIFILM). The heart was analysed in the two-dimensional mode in parasternal short-axis views. LV fractional shortening and ejection fraction were calculated using M mode imaging. To evaluate heart rate (HR) and velocity time integral (VTI), a pulsed Doppler of the LV outflow tract was performed, allowing calculation of stroke volume (SV = π × LV outflow radius^2 × VTI) and cardiac output (CO = SV × HR). LV outflow radius was measured for each animal. Aortic flow was measured using pulsed Doppler to verify the efficacy of transversal aortic constriction compared to sham mice. Echocardiographic analyses were performed with VevoLAB software.

Immunohistochemistry

Murine cardiac samples were sectioned into a central slice, which was snap-frozen. Cardiac sections were cut on a cryostat (8 µm thickness) and collected on SuperFrost plus glass slides.

After fixation in acetone for 10 min, non-specific binding sites were blocked in 3% BSA in PBS, followed by Biotin-Avidin Blocking kit (Thermo Scientific) when streptavidin (SA)-conjugates were used to detect biotinylated secondary antibodies. Primary antibodies (*see Suppl. Table 3*), diluted in 1% BSA in PBS, were incubated on the sections at r.t. for 1h, followed by repeated washing in PBS and incubation with secondary antibodies (*see Suppl. Table 3*) for 30 minutes to 1h. Double or triple stainings were performed sequentially, and negative controls included omission of primary antibodies. Slides were mounted in Vectashield containing DAPI, and images were acquired using x20 or x40 objectives on a Zeiss epifluorescence microscope (AxioImager J1) equipped with an apotome and Zen 2012 software (Zeiss). Images were analyzed by an operator blinded to the treatment groups using Fiji imaging software (NIH).

Suppl. Table 3 – antibodies used for immunohistochemistry in mice

antigen	article	supplier	species reactivity	host	dilution	Conc (µg/mL)
CD68	*14-0681-82*	eBioscience	*mouse*	**rat**	1/800	**5**
LYVE-1	*103-PA50*	Reliatech	*mouse*	**rabbit**	1/1000	**0.4**
Podoplanin	*14-5381-82*	eBioscience	*mouse*	**hamster**	1/10 000	**1**
IL-1β	*AF401NA*	RnD Systems	*mouse*	**goat**	1/100	**2**
WGA-FITC	*FP-CE8070*	Interchim			1/100	**1**
antigen	article	supplier		Fluorochrome		Conc (µg/ mL)
Donkey anti-Rabbit	*711-165-152*	Jackson Immunoresearch		**Cy3**		**3**
Streptavidin	*FP-CA5640*	Interchim fluoprobes		**Fluoprobe 647**		**0.7**
Biotinylated Donkey anti-Goat	*705-605-147*	Jackson Immunoresearch				**1.9**
Donkey anti-Rat	*712-586-152*	Jackson Immunoresearch		**Cy3**		**3**
Goat anti-Hamster	*A-21110*	Thermo Fisher Scientific Invitrogen		**AF488**		**0.8**

Image analysis of cardiac sections

Murine lymphatic vessels were defined as strongly Lyve1-positive structures, lacking macrophage markers (CD68), and mostly also positive for Podoplanin. Lymphatics are preferentially located in the subepicardium in rodent hearts. These Lyve1-positive, CD68-negative vessels clearly differ from $CD68^+$ macrophages, which either lack or display weaker Lyve1 expression. These macrophages, also differing in size and morphology from the elongated cell body and nucleus typical of lymphatic endothelial cells, were readily excluded from lymphatic counts. Photos were captured at *x20*.

Due to the absence of conclusive markers to distinguish precollectors from capillaries in murine cardiac lymphatics, we have made use of the fact that precollectors preferentially run in a base-to-apex fashion, whereas lymphatic capillaries lack such consistent spatial organization. Hence, by evaluating vessels with a lumen parallel to horizontal cardiac sections, the precollector population of vessels is more frequently detected as vessels running perpendicular to the section (= open lumen vessels). To assess the size and frequency of open lymphatic vessels (diameter > 5 µm; a population enriched in precollector vessels), between 10-20 images from the LV free-wall were collected and analyzed for each mouse. The density (open vessels/mm²) and lymphatic lumen sizes were measured and used to calculate mean

vessel diameter. The parameter % open lymphatic area was calculated as the sum total of all measured lymphatic diameters divided by the total cardiac area analyzed for each mouse heart. On average for each mouse 2.2±0.3 mm² of the LV was analyzed to determine lymphatic vessel sizes and % open lymphatic area.

Cardiomyocyte sizes were evaluated in sections double stained for CD31 and WGA imaged at *x40*. Cardiac macrophages were defined as CD68 positive cells. Infiltrating macrophages were defined as LYVE1$^-$ cells, and cardiac-resident macrophages as LYVE1$^+$ cells. Images were captured at *x20*.

Histology in mouse or human cardiac sections

Cardiac cryosections (8 µm) of mouse samples, or paraffin sections (5 µm) of human samples, were processed for Sirius Red staining, as described.[1] Cardiac interstitial collagen density was evaluated in mouse cardiac sections imaged on a light microscope (Zeiss) equipped with an *x40* objective. Replacement fibrosis (micro-scars) was evaluated in these images as total number per cardiac section of fibrotic hotspots, identified as images containing >11% fibrotic area per image, analyzing on average 14±0.5 images/sample (average total examined area 0.5 mm² of each LV cross-section). Perivascular fibrosis was evaluated in images taken at *x20,* focused on arterioles with a diameter range of 16-60 µm in both mice and men. On average 5 vessels/section were used to determine average fibrotic areas (µm²) per sample, which after normalization to lumen areas (µm²), was used to calculate "fibrotic ratio", as previously described.[4] Images were analyzed by an operator blinded to the treatment groups using Fiji imaging software (NIH).

Real-Time Polymerase Chain Reaction

Murine cardiac samples were collected at 8-weeks post-TAC. RNA extraction was performed with Trizol method. Briefly, samples were homogenized (45 sec.) in TRIZOL using Precellys tubes with beads. RNA was obtained after incubation, successively, in chloroform and isopropanol and three washes in ethanol. RNA quality was analyzed by Nanodrop 2000 (Thermo Fisher Scientific). cDNAs were generated using a reverse transcriptase after DNAse treatment. Real-time polymerase chain reaction was performed on a LightCycler 480 (Roche Molecular Biochemicals) with a commercially available mix (FastStart DNA Master SYBR Green I kit; Roche) on white 96-well plates. The reactions were performed in duplicate for each sample. Concentrations were calculated using a standard curve, obtained by serial dilutions of samples from an organ with high expression of the gene of interest. To normalize gene expression, values are expressed as ratios of a reference gene (E2F). Healthy sham animal ratios are then set as 100%, and values in TAC-operated animals are expressed relative to their respective sham controls. The sequences of the specific primers are detailed in *Suppl. Table 4*.

Suppl. Table 4 – list of primers used in mouse cardiac samples for qPCR

gene	sense	antisense	amplicon (bp)
Eef2	GCGAGGACAAAGACAAGGAG	GGGATGGTAAGTGGATGGTG	108
Ccl21	TCCCTACAGTATTGTCCGAGGC	ATCAGGTTCTGCACCCAGCCTT	141
Lyve1	ACCAGGTAGAGTCAGCGCAGAA	CAGGACACCTTTGCCATTCTTCC	128
Pdpn	ACAACCACAGGTGCTACTGGAG	GTTGCTGAGGTGGACAGTTCCT	116
Vegfc	AGCCCACCCTCAATACCAG	GCTGCTCCAAACTCCTTCC	154
Vegfd	CTCCACCAGATTTGCGGCAACT	ACTGGCGACTTCTACGCATGTC	112
Nppa	TACAGTGCGGTGTCCAACACAG	TGCTTCCTCAGTCTGCTCACTC	126
Nppb	TCCTAGCCAGTCTCCAGAGCAA	GGTCCTTCAAGAGCTGTCTCTG	98
Il1β	TGGACCTTCCAGGATGAGGACA	GTTCATCTCGGAGCCTGTAGTG	148
Il6	TACCACTTCACAAGTCGGAGGC	CTGCAAGTGCATCATCGTTGTTC	116
Il33	CTACTGCATGAGACTCCGTTCTG	AGAATCCCGTGGATAGGCAGAG	136

Western blot analysis in cardiac samples

Cardiac protein was extracted using Cell lysis buffer (#895347, RnD Systems) in microbead tissue dissociation tubes (Precellys #P000933-LYSK0-A – 0.5 mL). Twenty-five micrograms of denatured cardiac protein from healthy sham-operated or TAC-operated mice at 8 weeks post-TAC treated or not with anti-IL-1β antibodies, were separated on stain-free 4-20% agarose gels (Criterion TGX Precast Gel, Biorad), followed by blotting with a VEGFC antibody (#ab9546, Abcam; *1:1000*), or a VEGFD antibody (#ab155288, RnD systems; *1:500*), and finally an actin antibody (#15597191, Invitrogen; *1:10000*) diluted in PBS/BSA 5%. After repeated washing, HRP-conjugated secondary antibodies (goat anti-rat #sc-2006, Santa Cruz; *1:10000*, goat anti-rabbit #P0448, Dako; *1:5000*, donkey anti-mouse #A16011, Invitrogen; *1:5000*) were used. Target proteins were visualized using ECL chemiluminescence kit (#1705061, BioRad). Ratios of specific bands to actin signal per well was analyzed in ImageJ. For VEGF-C and VEGF-D multiple bands were present, representing the various cleaved forms of the growth factors. Total VEGF-C was calculated as the sum of the densities of full-length 31 kDa bands and cleaved, mature 21 kDa bands.[5] For VEGF-D only the full-length form (42 kDa) was visible (cleaved, mature form at 16 kDa too weak for analysis). VEGF-C and VEGF-D protein ratios were compared between sham and TAC groups using two-way ANOVA followed by Sidak's posthoc test.

Suppl. References

1. Heron, C. *et al.* Regulation and impact of cardiac lymphangiogenesis in pressure-overload-induced heart failure. *Cardiovasc. Res.* cvac086 (2022) doi:10.1093/cvr/cvac086.
2. Lygate, C. A. *et al.* Serial high resolution 3D-MRI after aortic banding in mice: band internalization is a source of variability in the hypertrophic response. *Basic Res. Cardiol.* **101**, 8–16 (2006).
3. Harouki, N. *et al.* The IL-1β Antibody Gevokizumab Limits Cardiac Remodeling and Coronary Dysfunction in Rats With Heart Failure. *JACC Basic Transl. Sci.* **2**, 418–430 (2017).
4. Dai, Z., Aoki, T., Fukumoto, Y. & Shimokawa, H. Coronary perivascular fibrosis is associated with impairment of coronary blood flow in patients with non-ischemic heart failure. *J. Cardiol.* **60**, 416–421 (2012).
5. Joukov, V. *et al.* Proteolytic processing regulates receptor specificity and activity of VEGF-C. *EMBO J.* **16**, 3898–3911 (1997).